

Pseudo Rotary Resonance Relaxation Dispersion Effects in Isotropic Samples

Authors: Evgeny Nimerovsky, Jonas Mehrens & Loren B. Andreas**

Affiliations:

Department of NMR based Structural Biology, Max Planck Institute for Multidisciplinary
Sciences, Am Faßberg 11, Göttingen, Germany

*Corresponding authors: land@mpinat.mpg.de ORCID: 0000-0003-3216-9065 and
evni@mpinat.mpg.de ORCID: 0000-0003-3002-0718.

Additional Experiments and Simulations

Spin-Lock (SL) simulations were performed using in-house MATLAB scripts based on
the numerical solution of the equation of motion.(Nimerovsky and Goldbourt, 2012) In the
simulations, two scenarios were considered in which the following external magnetic fields
gained additional time-dependent periodic terms from the rotation of the sample. The total
Hamiltonian is defined as:

$$H_{total} = H_{x\sim} + H_{B_1} \quad \text{with } x = \nu_0 \text{ or } \nu_1. \quad \text{Eqn. (S1)}$$

The simulated SL-signal is defined as follows:

$$S_{SL}(t_{SL}) = \int df \int dg \left[f(x)g(B_1)Tr \left\{ I_x \hat{T} e^{-i \int_0^{t_{SL}} dt H_{total}} I_x \hat{T} e^{i \int_0^{t_{SL}} dt H_{total}} \right\} \right], \quad \text{Eqn. (S2)}$$

where \hat{T} is a Dyson operator. The explicit forms of the $f(x)$ and $g(B_1)$ weighting factors are
shown below. The integrals in Eqn. (S2) were discretized sets, as shown in Figure S1.

1 $H_{\nu_0\sim}$ ($x = \nu_0$) represents a spatially inhomogeneous external magnetic field (first scenario),
2 which is described by the following eqn.:

$$H_{\nu_0\sim} = f(\nu_0)\Delta_{B_0,max} \sum_{n=1}^2 \cos(\omega_R t) I_z, \quad \text{Eqn. (S3A)}$$

3 where $f(\nu_0)$ represents a linear distribution function, varying from zero to 1 (shown in Figure
4 S1A) and also a weighting factor in Eqn. (S2). In simulations, we assumed that $\Delta_{B_0,max}$ (the
5 largest amplitude) reaches a value of 200 Hz. While we are qualitatively attempting to
6 understand the source of rotary-resonance condition for isotropic samples, this value is still
7 reasonable, as the ^{13}C peak width of the static sample was found to be around 440 Hz (Figure
8 S2A).

9 $H_{\nu_1\sim}$ ($x = \nu_1$) represents a spatially inhomogeneous rf-field (second scenario), which results in
10 time dependence of the amplitude of the SL. It is described by the following eqn.:

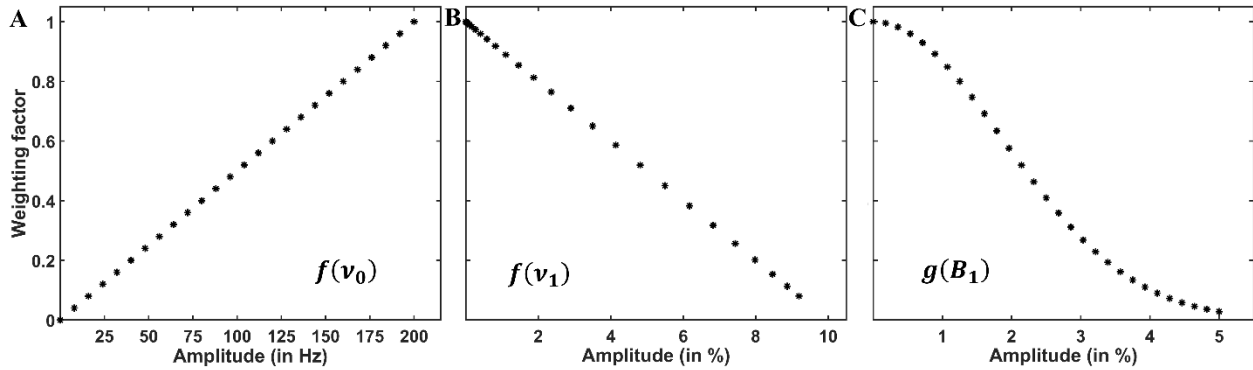
$$H_{\nu_1\sim} = 0.1\nu_{SL}(1 - f(\nu_1)) \sum_{n=1}^2 \cos(\omega_R t) I_y, \quad \text{Eqn. (S3B)}$$

11 where $f(\nu_1)$ is a biquadrate exponential distribution function (shown in Figure S1B) and also a
12 weighting factor in Eqn. (S2). ν_{SL} is applied rf-field strength. With this structure, the amplitude
13 varies from zero to approximately 9% relative to the applied ν_{SL} . While we are qualitatively
14 attempting to understand the source of rotary-resonance condition for isotropic samples, we did
15 not make any attempt to exactly simulate the rf-field distribution of the solenoidal coil. The
16 chosen distribution is still reasonable, based on the previous investigations of rf-field
17 inhomogeneity in NMR coils.(Idziak and Haeberlen, 1982; Kehlet et al., 2007; Tošner et al.,
18 2017, 2018)

1 H_{B_1} is the time-independent applied rf-field, which is also a distribution across the sample, and
 2 mainly accounts for the fact that a solenoidal coil produces a higher rf-field at the center, as
 3 compared with the edges:

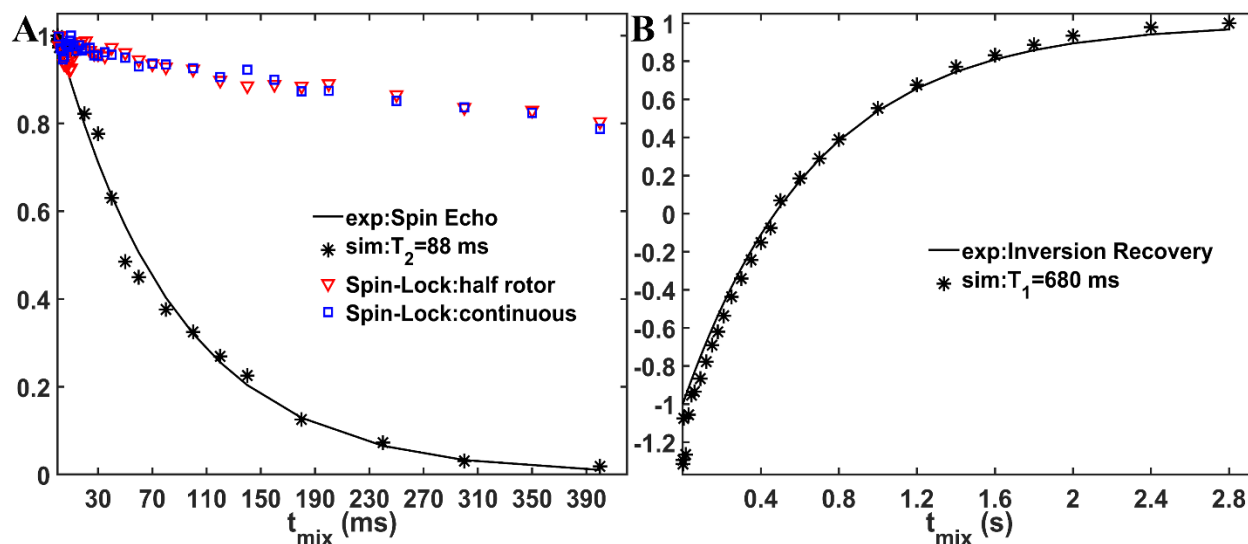
$$H_{B_1} = v_{SL}(1 - f_{B_1})I_x, \quad \text{Eqn. (S3C)}$$

4 where f_{B_1} is a linear distribution function, varying from 0 to 5% and $g(B_1)$ (in Eqn. (S2)) is a
 5 Gaussian weighting factor(Engelke, 2002; Gupta et al., 2015; Paulson et al., 2004; Xue et al.,
 6 2022) (shown in Figure S1C).



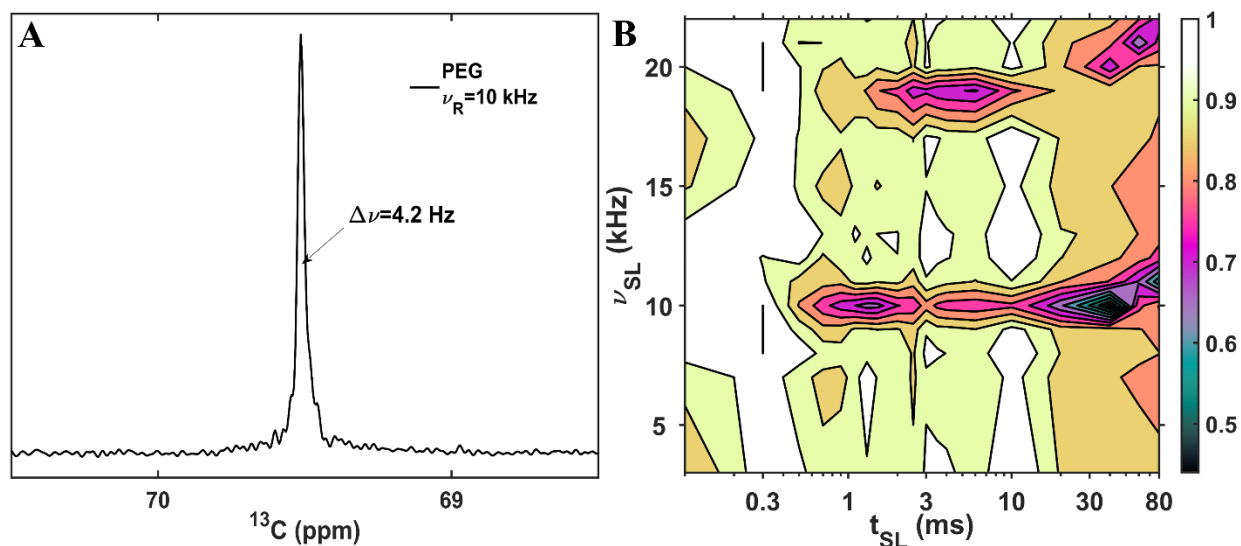
7 **Figure S1** The weighting factors for simulations of time-dependent periodic external magnetic field ($f(v_0)$, A) and
 8 rf-field ($f(v_1)$, B). (C) displays the weighting factor for time-independent rf-field inhomogeneity ($g(B_1)$).
 9

10 Figure S2A shows the comparison between experimental spin-echo curve(Hahn, 1950)
 11 (stars) and mono-exponential fitting (black line) with the obtained T_2 value of 88 ms from least-
 12 square fitting. Comparison of the experimental spin-lock curves with continuous (red triangles)
 13 and half-rotor-filled (blue squares) rf-field pulses show that the $T_{2\rho}$ value remains unchanged.
 14 Figure S2B shows the comparison between experimental inversion recovery curve(Vold et al.,
 15 1968) (stars) and mono-exponential fitting (black line) with the obtained T_1 value of 680 ms
 16 from least-square fitting.



1
 2 **Figure S2** ^{13}C $T_2 / T_{1\rho}$ (A) and T_1 (B) measurement for polybutadiene rubber. (A) The experimental spin-echo
 3 (stars) and mono-exponential fit (black line) at 20 kHz MAS. The red triangles and blue squares represent
 4 experimental spin-lock curves with continuous (at 10 kHz MAS) and half-rotor-filled (at 20 kHz MAS) rf-field
 5 pulses, respectively. For each case, 1 kHz rf-field strength was applied. (B) The experimental inversion recovery
 6 (stars) and mono-exponential (black line) curves at 20 kHz MAS.

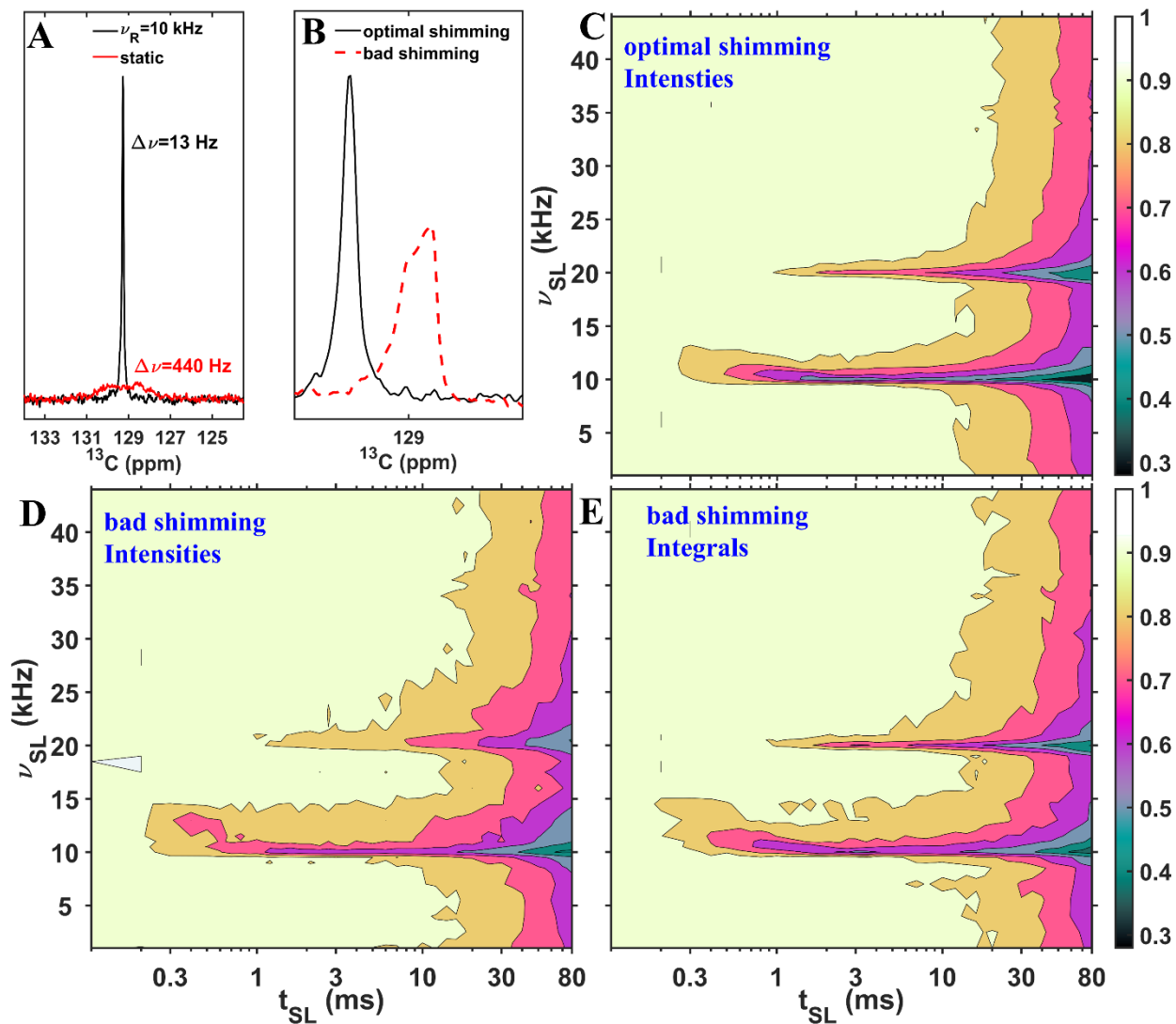
7 Figure S3A shows the 1D ^{13}C polyethylene glycol (PEG) signal under 10 kHz MAS.
 8 Figure S3B shows the SL profile, where two rotary-resonance conditions are observed at 10 kHz
 9 and ~ 20 kHz rf-field strengths.



10

1 **Figure S3** ^{13}C polyethylene glycol (PEG) experiments. (A) 1D spectrum recorded at 10 kHz MAS. (B) ^{13}C signal is
2 shown as a functions of the rf-field strength (ν_{SL} , y-axis) and mixing time (t_{SL} , x-axis) of the SL pulse.

3 Figure S4A shows the 1D ^{13}C spectrum of polybutadiene rubber at 10 kHz MAS (black)
4 and without spinning (red). Figure S4B shows the 1D ^{13}C spectrum of polybutadiene rubber at
5 10 kHz MAS with optimal (black) and deliberately degraded (red) shimming files. Figure S4C-E
6 shows SL profiles with optimal shimming (C, same as Figure 2A) and deliberately degraded (D
7 and E) shimming files. The same data is shown was used for D and E, and displayed either as
8 intensities (D) or integrals of the signal (E).



9

1 **Figure S4** ^{13}C spectra and SL profiles of polybutadiene rubber with different shims. (A) 1D signal at 10 kHz MAS
2 (black) and static (red). (B) 1D signal at 10 kHz MAS with optimal (black) and deliberately degraded (red)
3 shimming. (C-E) ^{13}C signal is shown as a functions of the rf-field strength (ν_{SL} , y-axis) and mixing time (t_{SL} , x-axis)
4 of the SL with optimal shims (C) and deliberately degraded shims (D and E). For (D) and (E), the same acquired
5 data was used; the difference is that in (D), the intensity is displayed, while in (E), the signal integral is shown.

6 **Sample preparation**

7 Commercial polybutadiene rubber with ^{13}C at natural abundance was cut in a single piece
8 to fill a 1.3 mm MAS rotor. A 4 mm MAS rotor was filled with 20 percent polyethylene glycol
9 solution in water with ^{13}C at natural abundance. Specifically, 26 mg of PEG was dissolved in
10 250 μL D_2O (10 %). This sample was filled in a 4 mm Bruker zirconium oxide (ZrO_2) rotor and
11 the cap was glued on top with two component epoxy to prevent leakage during spinning

12 **Solid NMR Spectroscopy**

13 *1.3 mm probe:* Spin-Lock experiments were conducted on a Bruker Avance III HD spectrometer
14 operating at 14.1 T (600 MHz ^1H frequency) using a DVT600W2 BL1.3 mm HXY probe. The
15 experiments were performed at static, 10, 20 and 35 kHz MAS. The temperature of the nitrogen
16 cooling gas set to 289 K, with 300 liters per hour. For decoupling of the heteronuclear j-
17 coupling, WALTZ-16 was used:(Shaka et al., 1983) 80 μs $2\text{-}\pi$ pulses (12 kHz rf-field strength).
18 In each experiment, 56 scans were recorded. The delay time between single experiments was set
19 to 2 s. For determination of the reference rf-field ^{13}C power, the 1D ^{13}C signal was recorded as a
20 function of the length of a single pulse (on resonance).

21 *4mm probe:* Spin-Lock experiments were conducted on a Bruker Avance III HD spectrometer
22 operating at 14.1 T (600 MHz ^1H frequency) using a 4 mm HXY probe. The experiments were
23 performed at 10 kHz MAS. The temperature of the nitrogen cooling gas was set to 290 K, with

1 300 liters per hour. SW_f-TPPM was used for decoupling of the heteronuclear j-coupling:(Thakur
2 et al., 2006) 120 μs for single ~π-pulse and 6.3 kHz rf-field strength. In each experiment, 64
3 scans were recorded. The delay time between single experiments was set to 2 s. For
4 determination of the reference rf-field ¹³C power, 1D ¹³C signal was recorded as a function of the
5 length of a single pulse.

6 REFERENCES

- 7 Engelke, F.: Electromagnetic wave compression and radio frequency homogeneity in NMR
8 solenoidal coils: Computational approach, *Concepts Magn. Reson.*, 15, 129–155,
9 <https://doi.org/10.1002/cmr.10029>, 2002.
- 10 Gupta, R., Hou, G., Polenova, T., and Vega, A. J.: RF Inhomogeneity and how it Control
11 CPMAS, *Solid State Nucl. Magn. Reson.*, 72, 17–26,
12 <https://doi.org/10.1016/j.ssnmr.2015.09.005>, 2015.
- 13 Hahn, E. L.: Spin Echoes, *Phys. Rev.*, 80, 580–594, <https://doi.org/10.1103/PhysRev.80.580>,
14 1950.
- 15 Idziak, S. and Haeberlen, U.: Design and construction of a high homogeneity rf coil for solid-
16 state multiple-pulse NMR, *J. Magn. Reson.* 1969, 50, 281–288, [https://doi.org/10.1016/0022-](https://doi.org/10.1016/0022-2364(82)90058-0)
17 [2364\(82\)90058-0](https://doi.org/10.1016/0022-2364(82)90058-0), 1982.
- 18 Kehlet, C., Bjerring, M., Sivertsen, A. C., Kristensen, T., Enghild, J. J., Glaser, S. J., Khaneja,
19 N., and Nielsen, N. Chr.: Optimal control based NCO and NCA experiments for spectral
20 assignment in biological solid-state NMR spectroscopy, *J. Magn. Reson.*, 188, 216–230,
21 <https://doi.org/10.1016/j.jmr.2007.06.011>, 2007.
- 22 Nimerovsky, E. and Goldbourt, A.: Insights into the spin dynamics of a large anisotropy spin
23 subjected to long-pulse irradiation under a modified REDOR experiment, *J. Magn. Reson.*, 225,
24 130–141, <https://doi.org/10.1016/j.jmr.2012.09.015>, 2012.
- 25 Paulson, E. K., Martin, R. W., and Zilm, K. W.: Cross polarization, radio frequency field
26 homogeneity, and circuit balancing in high field solid state NMR probes, *J. Magn. Reson.*, 171,
27 314–323, <https://doi.org/10.1016/j.jmr.2004.09.009>, 2004.
- 28 Shaka, A. J., Keeler, J., Frenkiel, T., and Freeman, R.: An improved sequence for broadband
29 decoupling: WALTZ-16, *J. Magn. Reson.* 1969, 52, 335–338, [https://doi.org/10.1016/0022-](https://doi.org/10.1016/0022-2364(83)90207-X)
30 [2364\(83\)90207-X](https://doi.org/10.1016/0022-2364(83)90207-X), 1983.

- 1 Thakur, R. S., Kurur, N. D., and Madhu, P. K.: Swept-frequency two-pulse phase modulation for
2 heteronuclear dipolar decoupling in solid-state NMR, *Chem. Phys. Lett.*, 426, 459–463,
3 <https://doi.org/10.1016/j.cplett.2006.06.007>, 2006.
- 4 Tošner, Z., Porea, A., Struppe, J. O., Wegner, S., Engelke, F., Glaser, S. J., and Reif, B.:
5 Radiofrequency fields in MAS solid state NMR probes, *J. Magn. Reson.*, 284, 20–32,
6 <https://doi.org/10.1016/j.jmr.2017.09.002>, 2017.
- 7 Tošner, Z., Sarkar, R., Becker-Baldus, J., Glaubitz, C., Wegner, S., Engelke, F., Glaser, S. J., and
8 Reif, B.: Overcoming Volume Selectivity of Dipolar Recoupling in Biological Solid-State NMR
9 Spectroscopy, *Angew. Chem. Int. Ed.*, 57, 14514–14518,
10 <https://doi.org/10.1002/anie.201805002>, 2018.
- 11 Vold, R. L., Waugh, J. S., Klein, M. P., and Phelps, D. E.: Measurement of Spin Relaxation in
12 Complex Systems, *J. Chem. Phys.*, 48, 3831–3832, <https://doi.org/10.1063/1.1669699>, 1968.
- 13 Xue, K., Nimerovsky, E., Tekwani Movellan, K. A., Becker, S., and Andreas, L. B.: Backbone
14 Torsion Angle Determination Using Proton Detected Magic-Angle Spinning Nuclear Magnetic
15 Resonance, *J. Phys. Chem. Lett.*, 13, 18–24, <https://doi.org/10.1021/acs.jpcclett.1c03267>, 2022.

16

17